Diagnostic technique for measuring fusion reaction rate for inertial confinement fusion experiments at Shen Guang-III prototype laser facility*

Wang Feng(王 峰)[a)†], Peng Xiao-Shi(彭晓世)[a)], Kang Dong-Guo(康洞国)[b)], Liu Shen-Ye(刘慎业)[a)], and Xu Tao(徐 涛)[a)]

[a)] *Research Center of Laser Fusion, Chinese Academy of Engineering Physics, Mianyang* 621900, *China*
[b)] *Institute of Applied Physics and Computational Mathematics, Beijing* 100088, *China*

(Received 24 October 2012; revised manuscript received 27 April 2013)

A study is conducted using a two-dimensional simulation program (Lared-s) with the goal of developing a technique to evaluate the effect of Rayleigh–Taylor growth in a neutron fusion reaction region. Two peaks of fusion reaction rate are simulated by using a two-dimensional simulation program (Lared-s) and confirmed by the experimental results. A neutron temporal diagnostic (NTD) system is developed with a high temporal resolution of ~ 30 ps at the Shen Guang-III (SG-III) prototype laser facility in China, to measure the fusion reaction rate history. With the shape of neutron reaction rate curve and the spherical harmonic function in this paper, the degree of Rayleigh–Taylor growth and the main source of the neutron yield in our experiment can be estimated qualitatively. This technique, including the diagnostic system and the simulation program, may provide important information for obtaining a higher neutron yield in implosion experiments of inertial confinement fusion.

Keywords: inertial confinement fusion, Rayleigh–Taylor growth, neutron fusion reaction, implosion

PACS: 52.57.Fg, 42.87.–d, 52.57.–z **DOI:** 10.1088/1674-1056/22/11/115204

1. Introduction

In implosion experiments of inertial confinement fusion (ICF), shells filled with deuterium (D2) or a deuterium–tritium (DT) mixture are heated by either direct laser illumination or soft x-ray radiation in a laser-heated Hohlraum.[1–6] The target is compressed to conditions under which thermonuclear fusion occurs. For the diagnostic technique, several detectors measuring the neutron bang time have been described in the literature,[1–4] but only the streak camera–based neutron temporal diagnostic (NTD) system is capable of resolving the details of the neutron burn history with a resolution of ~ 30 ps for DT neutrons.

Time history of neutron reaction rate with two peaks has been observed in the collapse of asymmetrically driven convergent shock in direct-drive experiment with spherical plastic (CH) capsules.[7] The capsules were filled with an equimolar (by atom) mixture of D_2 and helium-3(^{3}He) gas and had an initial density of 2.5 mg/cm^3.

Target and laser illumination nonuniformities can feed through to the inner surface of the shell in the deceleration phase. Amplified by the Rayleigh–Taylor (RT) growth, these nonuniformities could severely disrupt the hot, neutron-producing region of the target, leading to a strongly distorted neutron burn history.[1,2] With the increase of the roughness degree, the neutron yield decreased in the Nova implosion experiment.[8]

In the present paper, the NTD system is set up on the Shen Guang-III (SG-III) prototype laser facility in China. The two-peak time history of the neutron reaction rate is observed with a time resolution of ~ 30 ps for the first time in China under a neutron yield of about 10^{10} on room-temperature indirect-drive implosion. The two-peak shape on the time scale has been explained qualitatively with the Lared-s program[9] and confirmed by the experimental results. The first peak, called the "shock peak", shows the shock wave compression caused by the ablation. And the second peak, called the "inertial peak", shows the shock wave compression caused by the shock wave reflected by the interface of SiO_2 and DT.

After the comparison between the experimental results and the simulation curve with Lared-s program, the disturbance effect of the Rayleigh–Taylor growth in the implosion experiment could be estimated qualitatively. With the Rayleigh–Taylor growing, the highest value of the "inertial peak" and its relevant neutron yield, which is the area of the "inertial peak" curve, are smaller than those in the "shock peak" case. This paper provides a valuable technique to evaluate and analyze the effect of Rayleigh–Taylor growth in fusion reaction experiments for inertial confinement fusion studies.

*Project supported by the National Natural Science Foundation of China (Grant No. 10805041), the Science and Technology on Plasma Physics Laboratory, China (Grant No. 9140C6801021001), and the Science and Technology Development Foundation of China Academy of Engineering Physics, China (Grant No. 2011B0102020).

†Corresponding author. E-mail: xiaozei7566@163.com

© 2013 Chinese Physical Society and IOP Publishing Ltd

2. Two-shock compression simulation

In this section, we first introduce the simulation results with the two converging shocks. Then, we use the spherical harmonic function to simulate the non-uniformity effect on the time shape of the fusion reaction rate and neutron yield in an implosion experiment.

In our indirect drive experiment, the target structure in Fig. 1 is the multilayer with CH-SiO_2-DT. Due to the shell process, there are some nonuniformities in the CH layer, which may cause Rayleigh–Taylor growth in a fusion reaction experiment. A SiO_2 ball should hold about 10^6 Pa DT of fuel material. In order to analyze the history of reaction rate, we simulate the neutron reaction with the two-dimensional Lared-s[9] program for a CH-SiO_2-DT structure as shown in Fig. 2.

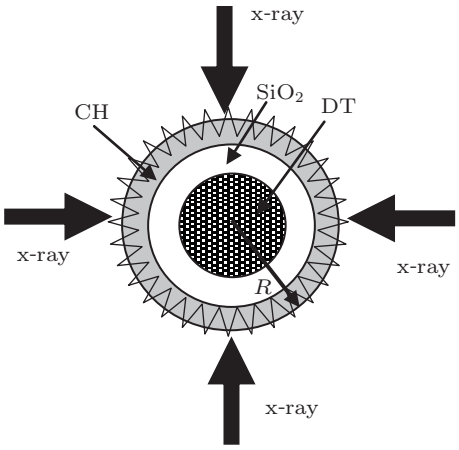


Fig. 1. Diagram of the CH-SiO_2-DT target for the indirect drive experiment.

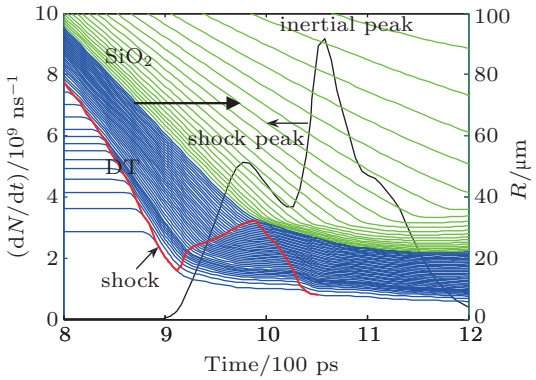


Fig. 2. Stream lines of two-shock-wave compression with a CH-SiO_2-DT target. dN/dt and R present the fusion reaction rate and the radius of the fuel target in Fig. 1, respectively.

In Fig. 2, the stream lines with green and blue colors show the compressing SiO_2 and DT material, respectively. The red line indicates the shock front in DT material which is reflected by the interface between DT and SiO_2 many times. The black line shows the fusion reaction rate in the simulation program. The area below the black lines denotes the neutron yield. The first peak of black line, called the "shock peak", shows the shock wave compression caused by the CH ablation. The second peak of the black line, called the "inertial peak", shows the shock wave compression which is caused by the shock wave reflected by the interface between SiO_2 and DT. In the simulation program, the first peak ("shock peak") is lower than the second peak ("inertial peak").

From the fusion reaction rate in Fig. 2, the black line shows the ideal shape of fusion reaction rate. As is well known, target and laser illumination nonuniformities can feed through to the inner surface of the shell in the deceleration phase. Amplified by the Rayleigh–Taylor growth, these nonuniformities can severely disrupt the hot, neutron-producing region of the target, leading to a strongly distorted neutron burn history. As a simulation improvement for Fig. 2, we can use the spherical harmonic function to simulate the non-uniformity effect on the time shape of the fusion reaction rate and the neutron yield in an implosion experiment.

As a qualitative approach, the disturbance on the shell surface can be unwrapped with a spherical harmonic function about mode numbers 4–24. Therefore, there are two parameters that can be added to spherical harmonic function, which are phase modulation and disturbance amplitude.

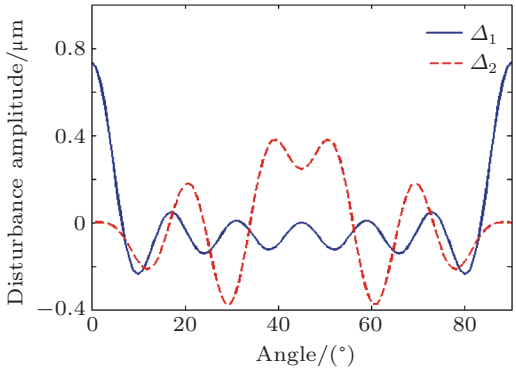


Fig. 3. Variations of disturbance amplitudes with angle of the spherical harmonic for two cases.

Figure 3 shows that the disturbance amplitude (RMS = 0.3 μm) changes with the spherical harmonic angle for the cases with phase modulation (Δ_2) and without phase modulation (Δ_1). The expression without phase modulation is

$$\Delta_1 = \sum_L A_L \cos(L\theta), \quad L = 4, 8, \ldots, 24, \tag{1}$$

where Δ_1 is the parameter for "without" phase modulation, A_L is the amplitude with mode number L, and θ is the angle of the spherical harmonic function.

The expression with phase modulation is

$$\Delta_2 = \sum_{L=8,16,20} A_L \cos(L\theta) + \sum_{L=4,12,24} A_L \cos(L\theta + \pi), \tag{2}$$

where Δ_2 is the parameter for "with" phase modulation, the parameters of A_L, L, and θ are the same as those in formula (1). The disturbance amplitude is given by the root mean square value (RMS), i.e., RMS $= \sqrt{\sum_L A_L}$.

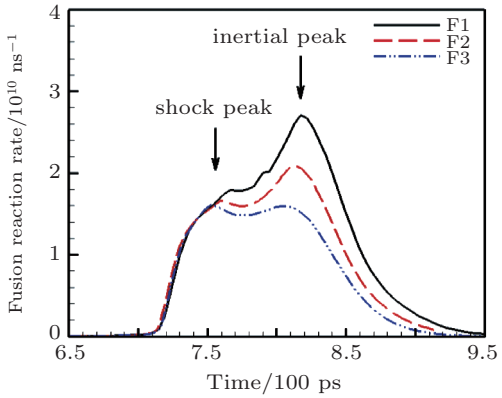


Fig. 4. Variations of fusion neutron rate and yield with time.

Figure 4 shows the simulation results using phase modulation and disturbance amplitude in a two-dimensional program (Lared-s) under the experimental target condition. The area under the curve represents the fusion neutron yield. It is very clear that there is a "shock peak" and a "inertial peak", as explained in Fig. 2. F1 shows the results in the case with neither disturbance nor phase modulation. F2 shows the results in the case with disturbance but no phase modulation. F3 shows the results in the case with both disturbance and phase modulation. These are the low-quality data, which means the nonuniformity amplified by the Rayleigh–Taylor growth in the target region can severely disrupt the hot, neutron-producing region of the target. Since the area below the curve in Fig. 4 represents the neutron yield, the neutron yield of curve shape F3 is lowest.

3. Diagnostic layout and experimental results

The NTD system, shown schematically in Fig. 5, has three parts, i.e., scintillator, optical system, and recording system.[2] A fast plastic scintillator (EJ-232, rising time $<$ 30 ps) converts the kinetic energy of the neutrons into light. A light collection and transfer system transfers the light from the scintillator to the input plane of a fast ($<$ 10 ps) optical streak camera. The front end of the optical system is inserted close to the target. An optical fiducial is used to show the time of the neutron signals relative to the incident laser pulse. The fiducial system provides cross timing between the neutron signal and incident laser pulse, which is recorded on the streak camera. The neutron number (i.e., neutron yield for one burn) that enables the scintillator to record high-quality burn histories is about 10^{10}. The scintillator with 6-mm diameter and 1-mm thickness is placed at 2 cm, the distance from the target to the required standoff. Due to the limited size of the photocathode of the optical streak camera (OSC), a demagnifying optical system with a 3:1 ratio is used.

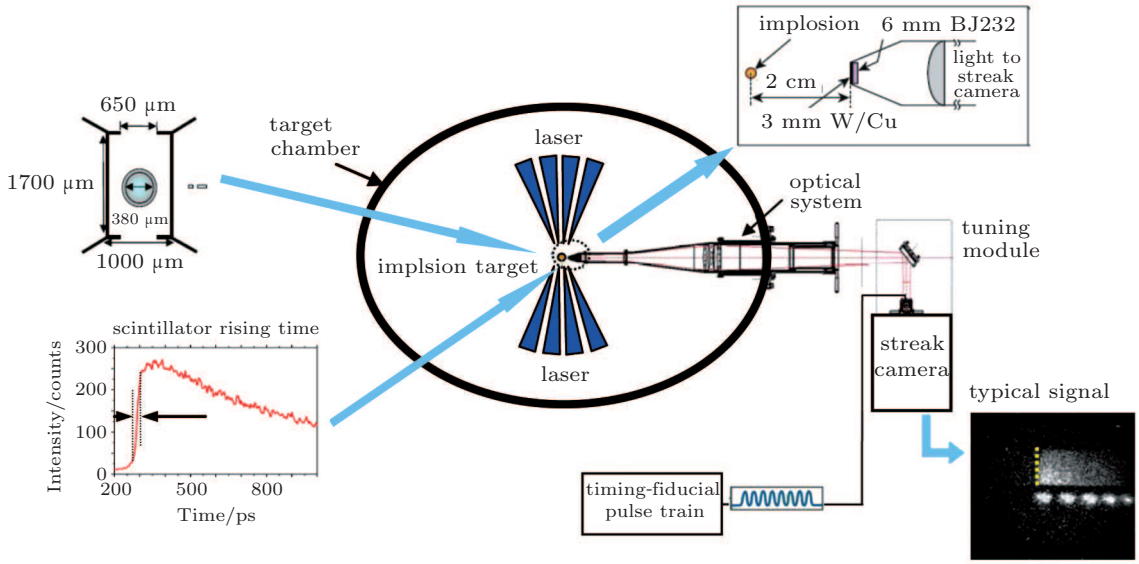


Fig. 5. A block diagram of NTD detector system integrated into the SG-III prototype.

Figure 6 shows the signal image and the data averaged across the central portion of the scintillator signal. The fiducial is seen at the bottom of the image and the scintillator output signal in the center. The streak camera flat-field and geometric distortions are included in the signal processing. The time history of the scintillator signal is the convolution of the neutron temporal distribution with the scintillator response. The scintillator has a very fast rise time of $<$ 20 ps and a decay time of $\sim$ 1.2 ns. Consequently, the burn history information is encoded in the leading edge of the pulse due to the fact that the decay time of the scintillator is much longer than the burn width. The time space of each fiducial point is 500 ps used as a time scale, which is recorded on the streak camera. With the fiducial, the time relation among different experiments can be calibrated.

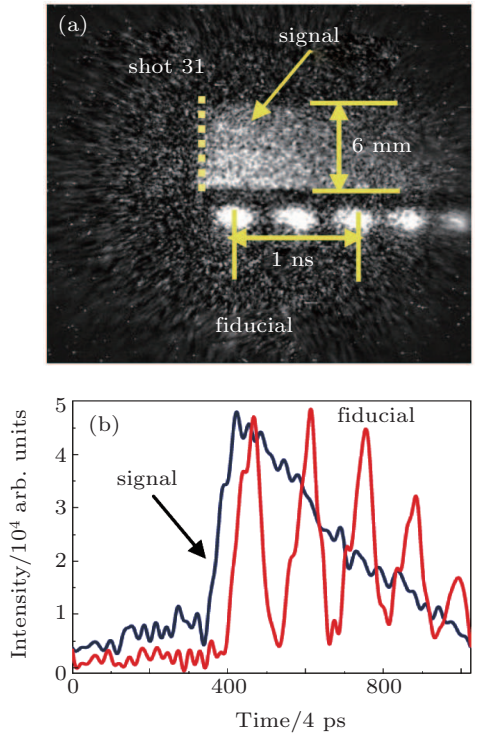


Fig. 6. Signal and analysis of laser pulse for shot 31. (a) Signal and fiducial of experimental result with 13-μm thick CH material and (b) comparison of time between signal and fiducial.

The actual neutron burn history is obtained by deconvolving the effect of the long scintillator decay from the recorded signal. A "physical modeling" approach is used for the deconvolution[2]

$$n_i = s_i - \sum_{j=0}^{i-1} n_j \exp\left(\frac{t_i - t_j}{\tau}\right), \tag{3}$$

where the neutron signal n_i at the pixel location i is given as the recorded signal s_i minus the sum of all earlier neutron signals, which are decaying exponentially at the scintillator fall time τ, and t_i and t_j represent the times in the experimental image.

This method is fast, deterministic, and is very stable against noise on the streak camera signal. The neutron signal is broadened by several different mechanisms. The thermal broadening of the neutron energy spectrum leads to an arrival time spread in the scintillator.

With formula (3), the time history of the neutron reaction rate is obtained as shown in Fig. 7. There are two parameters of shape and area which should be analyzed if we compare Fig. 7 with Fig. 4. The first peak for each of the three shots (shot 30, shot 31, and shot 32) is higher than the second peak. However, the first peak is lower than the second peak with 19-μm thick CH (shot 28). The area ratio between the two peaks is shown in the inset.

In order to analyze the experimental results, we simulate the time history of the neutron reaction rate with the Lared-s program under the ideal condition (without Rayleigh–Taylor growth) for different CH thicknesses (see Fig. 8). In Fig. 8, the shock peak is lower than the inertial peak for the 9-μm thick CH. This is consistent with the result of shot 30 in Fig. 7.

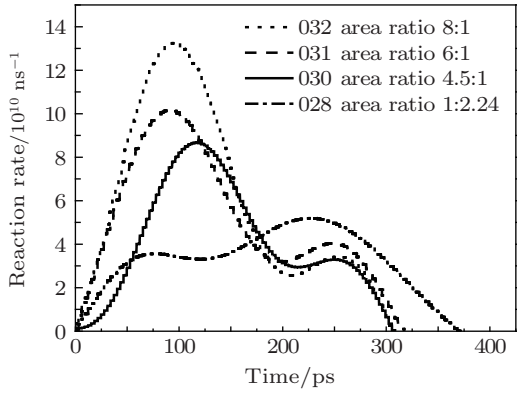


Fig. 7. Time histories of the neutron reaction rate with shot 28, shot 30, shot 31, and shot 32. The ablation layers are 19-μm thick CH, 9-μm thick CH, 13-μm thick CH, and 16-μm thick CH materials, respectively.

In Fig. 8, the first peak value of dashed line (Δ_{CH} = 13 μm) is lower than that of dotted line (Δ_{CH} = 16 μm). This trend is confirmed with the results of shot 31 (13-μm thick CH) and shot 32 (16-μm thick CH) in Fig. 7. From the changes of F1, F2, and F3 in Fig. 4, we find that the effect of RT growth on the second peak is more serious than on the first peak. Thus, it can be explained why the second peaks of shot 31 and shot 32 in Fig. 7 are lower than the first peak .

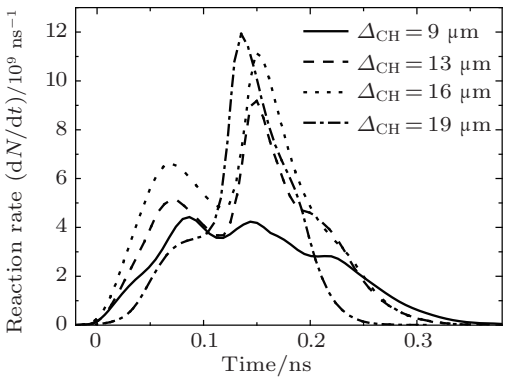


Fig. 8. Simulation time histories of neutron reaction rate with the Lared-s program under the ideal condition for different CH thickness values.

In Fig. 8, the dash-dot line shows the curve with 19-μm thick CH. The second peak is higher than the first peak. In our opinion, there are two possible reasons for the shot 28 curve. The first reason is the RT effect, and the second one is the inertial peak value. Since the 19-μm thick CH is thickest in the four experiments, the effect of the RT growth may be the smallest (no other effects). And because the second peak value of dash-dot line is highest in Fig. 8 in the four simulation lines, the decreasing of inertial shock should be smallest in the four experiments. Therefore, the shot 28 curve is different from the other curves. In addition, the inertial peak is higher than the shock peak.

After a comparison of the experimental results (Fig. 7) and the simulation data (Figs. 2, 4, and 8), we find that the nonuniformity (disturbance and phase modulation in program) in the DT shell and laser illumination may be the main reason for the low neutron yield of the neutron reaction. The time history of the neutron reaction rate can give us very important information about the degree of the neutron reaction. If the first peak is higher than the second peak, the neutron yield may be mainly generated by the first shock wave compression. If the first peak is lower than the second peak, the neutron yield may be mainly generated by the second shock wave compression. Figures 4 and 8 show that the high neutron yield will occur when the second peak is higher than the first peak. So we should control the shell and laser illumination uniformity to approach to the ideal shape of time history.

4. Discussion

From the experimental results and simulation data in this paper, we find some useful information about understanding the neutron reaction ratio and Rayleigh–Taylor instability. The Rayleigh–Taylor instability could affect the neutron reaction ratio. From the shape of the neutron reaction ratio, the effect of Rayleigh–Taylor growth in our experiment can be regarded as the sphere harmonic function in the Lard-s program (Figs. 3 and 4). However, these explanations did not consider the difference in CH ablation thickness. Thus, we should analyze the relationship between the Rayleigh–Taylor growth and the CH ablation thickness in our experimental results.

From some literatures,[1,10] the growth factor γ of Rayleigh–Taylor is directly related to the acceleration factor a, which is related to the ablation layer thickness.[10–12] As the thickness increases, the growth factor γ becomes smaller because the mass in the shell is heavier. From our experimental data, the curve shapes and the highest values in Fig. 7 for shot 32 (16 μm), shot 31 (13 μm), and shot 30 (9 μm) are almost similar. It can be found that the Rayleigh–Taylor instability is not the core factor in our experiment, and the growth factor γ for shot 28 (19 μm) is lowest due to the larger thickness when the shell targets are fabricated with the same technology in this experiment. Then, the curve shapes and the areas below the curves in Fig. 7 can be explained mainly by the simulation curves in Figs. 2–4.

5. Conclusion

In summary, a neutron temporal diagnostic (NTD) system is developed for the SG-III prototype in China for the first time to allow the high resolution measurement of the neutron burn history on early in-drive DT targets. This instrument is able to measure the neutron burn history for yield $> 10^{10}$ DT neutrons with a resolution of ~ 30 ps. A two-time compression is found from the time history of the neutron reaction rate. The high neutron yield should be mainly generated by the second shock wave compression in Fig. 2. The smaller the Rayleigh–Taylor growth in the neutron reaction region, the more similar to the F1 in Fig. 4 the shape of reaction rate curve is.

With the shape of the reaction rate curve and the spherical harmonic function in Figs. 2–4, we can estimate the degree of the Rayleigh–Taylor growth effect and the main source of the neutron yield in our experiment. This new technique, including the diagnostic system and the simulation program, may provide important information about obtaining a higher neutron yield in implosion experiments of inertial confinement fusion.

References

[1] Lindl J D, Amendt P, Berger R L, Glendining S G, Glenzer S H, Hann S W, Kauffman R L, Landen O L and Suter L J 2004 *Phys. Plasmas* **11** 339

[2] Stoeckl C, Glebov V Y, Roberts S and Sangster T C 2003 *Rev. Sci. Instrum.* **74** 1713

[3] Lerche R A and Cable M D 1996 UCRL-LR-105821-96-3

[4] Moran M J, Lerche R A and Mant G 2006 *Rev. Sci. Instrum.* **77** 10E718

[5] Mack J M, Caldwell S E, Evans S C, Sedillo T J, Wilson D C, Young C S, Horsfield C J, Griffith R L and Lerche R A 2006 *Rev. Sci. Instrum.* **77** 10E728

[6] Lerche R A, Phillion D W and Tietbohl G L 1995 *Rev. Sci. Instrum.* **66** 933

[7] Rygg J R, Frenje J A, Li C K, Seguin F H, Petrasso R D, Marshall F J, Delettrez J A, Knauer J P, Meyerhofer D D and Stoeckl C 2008 *Phys. Plasmas* **15** 034505

[8] Dittrich T R, Hammel B A, Keane C J, McEachern R, Turner R E, Hann S W and Suter L J 1994 *Phys. Rev. Lett.* **73** 2324

[9] Fan Z F, Xue C, Wang L F, Ye W H and Zhu S P 2011 *Phys. Plasmas* **18** 062108

[10] Zhang J and Chang T Q 2004 *Fundaments of the Target Physics for Laser Fusion* (Beijing: National Defence Industrial Press) p. 257

[11] Jiang S E, Miao W Y and Kuang L Y 2011 *Acta Phys. Sin.* **60** 055206 (in Chinese)

[12] Tao Y S, Wang L F, Ye W H, Zhang G, Zhang J C and Li Y J 2012 *Acta Phys. Sin.* **61** 075207 (in Chinese)